# Thermoelastic Kirchhoff Plate: An Analytical Model for Shot Peen Forming of Metal Panels

Conor Rowan *
*University of Colorado Boulder, Boulder, CO, 80303*

**Metal wing skin panels are planar structure that cover the rib and stringer assemblies on either side of the wingbox. Because the wing is not rectangular, skin panels, which are machined from plate stock, must be contoured to match the wing geometry. A common technique used in factories is shot peen forming, where the panel is sprayed with a high-velocity stream of small steel pellets called shot. The impacts between the hard steel shot and softer aluminum panel cause localized plastic deformation, both improving the fatigue properties of the material's surface and imparting a residual stress distribution that results in bending. Thus, a torque is associated with the through-thickness shot peen stress distribution. Shot peen forming is conceptualized as the application of spatially varying torques, which are modeled with the input of applied temperatures. In this paper, we derive the bending equations for a thermally loaded homogeneous Kirchhoff plate. A simple test is devised to extract the value of an equivalent applied torque from the bending response of uniformly shot peened plates, which circumvents the difficulty of accounting for surface plasticity. This torque can be used as an input to the theoretical model to predict the shape of rectangular plates under more complicated shot peen conditions. An experiment is designed and carried out which investigates the agreement between the model and real shot peen operations. The effect of uncertainty in the experiment is estimated with Monte Carlo methods.**

## I. Nomenclature

| | | |
|---|---|---|
| $\epsilon_{ij}$ | = | strain tensor |
| $\sigma_{ij}$ | = | stress tensor |
| $x_i$ | = | spatial coordinates |
| $u_i$ | = | displacement in $x_i$ direction |
| $T$ | = | temperature field |
| $p_3$ | = | transverse pressure |
| $\Pi$ | = | energy functional |
| $P_n$ | = | $n$-th order Legendre polynomial |
| $E$ | = | Young's modulus |
| $\nu$ | = | Poisson's ratio |
| $G$ | = | shear modulus |
| $\alpha$ | = | coefficient of thermal expansion |
| $h$ | = | plate thickness |
| $L_1$, $L_2$ | = | plate side lengths |

## II. Introduction

Past attempts to quantitatively model shot peen forming have relied entirely on complex Finite Element models. Koch [1] simulated individual panel/shot collisions and superimposed the resultant strain distributions as an input to a metal panel modeled in ABAQUS. Wang, Platts, and Levers [2] used measurements from test samples to match the through-thickness stress distribution of shot peened parts using a thermal model in ABAQUS. Both methods explicitly model surface plasticity with applied temperatures and can take multiple days to run. Additionally, they do not permit predictions of shot peen forming recipes for given contour requirements because they are non-linear and

*PhD Student, Aerospace Engineering

thus non-invertible. Nervi and Castle [3] develop a general model to analyze distortion of thin aerospace components, but focus on machining processes and do not clearly found their approach in plate theory. Furthermore, they do not focus on the analytical solution methods which would be necessary to further develop shot peen specific modeling. Here, an analytical thermoelastic model is proposed where simple tests can relate shot peening at a given intensity to equivalent through-thickness temperature distributions. **It is here stressed that thermoelasticity is chosen as a convenient modeling framework, not as an attempt to faithfully capture the physics of shot peening.** Distortion from shot peen is driven by plastic impacts, and the goal of the thermal model is to capture the bending distortion without modeling plasticity or impacts. As will be seen, this approach manages to be effective while avoiding long run times and non-invertibility, which are consequences of plasticity. Skin panels are modeled as isotropic Kirchhoff plates [4], and the moment associated with the equivalent temperature distribution is used as an input to a plate bending problem which relates thermal and pressure loading to the transverse displacement field. Plasticity is not incorporated, as the through-thickness stress/strain distribution is not chosen to match that of a peened panel. **The hypothesis is that a plate's bending response to shot peening is accurately modeled by the application of a bending moment distribution whose magnitude is fit to the shot peen process with a factory test. Thermoelasticity is useful here as a means of using established theory to apply distributed bending moments to a plate, which is not a typical load case. In other words, shot peen deformations are modeled with thermoelasticity but are not driven by an actual thermal process.** The governing equations for the thermoelastic plate are solved for unconstrained edges using the Rayleigh-Ritz method. A method for solving the inverse problem of predicting forming conditions from a specified displacement field is also presented. Finally, an experiment is designed and carried out in order to assess the validity of the theoretical developments.

## III. Thermoelastic Plate Model

By assumption, all strain components involving the 3 index (through-thickness direction, see Figure 1) are zero in the Kirchhoff plate. The general relationship between stress and in-plane strains for an isotropic, thermoelastic material is:

$$\epsilon_{11} = \frac{1}{E}\Big(\sigma_{11} - \nu\sigma_{22}\Big) + \alpha T$$

$$\epsilon_{22} = \frac{1}{E}\Big(\sigma_{22} - \nu\sigma_{11}\Big) + \alpha T$$

$$\gamma_{12} = 2\epsilon_{12} = \frac{1}{G}\sigma_{12}$$

Mechanical plate strains are viewed as arising from a combination of stresses and an applied temperature distribution $T = T(x_1, x_2, x_3)$. The tensorial shear strain $\epsilon_{12}$ is distinguished from its "engineering" counterpart $\gamma_{12}$. Inverting this relationship, stresses can be written in terms of mechanical plate strains and the temperature:

$$\sigma_{11} = \frac{E}{1-\nu^2}\Big(\epsilon_{11} + \nu\epsilon_{22}\Big) - \frac{E\alpha T}{1-\nu} \tag{1a}$$

$$\sigma_{22} = \frac{E}{1-\nu^2}\Big(\epsilon_{22} + \nu\epsilon_{11}\Big) - \frac{E\alpha T}{1-\nu} \tag{1b}$$

$$\sigma_{12} = G\gamma_{12} = \frac{E}{2(1+\nu)}\gamma_{12} = \frac{E}{(1+\nu)}\epsilon_{12} \tag{1c}$$

The shear modulus $G$ has been written in terms of $E$ and $\nu$. We employ the usual kinematic assumptions about plate bending–mechanical strains in the plate as a function of the angle of rotation of the normal material line, which can be written as a derivative of the transverse displacement $u_3$. Under the Kirchhoff assumptions, the $x_1$ displacement is $u_1(x_1, x_2) - x_3 u_{3,1}$ and the $x_2$ displacement is $u_2(x_1, x_2) - x_3 u_{3,2}$. The first terms are in-plane displacements and $u_3(x_1, x_2)$ is the transverse displacement field. This leads to the following form of strain:

$$\epsilon_{11} = \frac{\partial u_1}{\partial x_1} - x_3 \frac{\partial^2 u_3}{\partial x_1^2} \tag{2a}$$

$$\epsilon_{22} = \frac{\partial u_2}{\partial x_2} - x_3 \frac{\partial^2 u_3}{\partial x_2^2} \tag{2b}$$

$$\gamma_{12} = \frac{\partial u_1}{\partial x_2} + \frac{\partial u_2}{\partial x_1} - 2x_3 \frac{\partial^2 u_3}{\partial x_1 \partial x_2} \tag{2c}$$

Plate strains are functions of $x_3$ and derivatives of the displacement components $u_1$, $u_2$, and $u_3$, which depend on the in-plane coordinates $x_1$ and $x_2$ only. See [4] for a more complete derivation and further explanation. This form of strain can be substituted into the generalized Hooke's Law given in Eq. 1 to write the stress components in terms of the displacement field. We have assumed that the form of strain in the thermoelastic plate is identical to that of the usual Kirchhoff plate, but that the stresses arising from these mechanical strains have additional dependence on the temperature field. With these basic components of the thermoelastic plate, there are two routes to be taken. In the differential approach, governing equations can be derived using free body diagrams and force/moment balances. This is the method employed in the typical exposition of plate models. Alternatively, an energy and variational approach can be adopted, which will lend itself to more robust solution procedures. This is the integral formulation. Both approaches will be discussed, and the resulting governing equations will be shown to agree.

**A. Differential Formulation**

Using free body diagrams on differential plate elements leads directly to governing differential equations. The moment components, which are technically moment per width, arise from the in-plane plate stresses:

$$M_1 = -\int_h x_3 \sigma_2 dx_3 \tag{3a}$$

$$M_2 = \int_h x_3 \sigma_1 dx_3 \tag{3b}$$

$$M_{12} = -\int_h x_3 \sigma_{12} dx_3 \tag{3c}$$

Plugging Eqs. 2 into Eqs. 1, these integrals can be carried out and simplified with the introduction of a few definitions:

$$M_1 = D_1 \left( \frac{\partial^2 u_3}{\partial x_2^2} + \nu \frac{\partial^2 u_3}{\partial x_1^2} \right) + D_2 \tau \tag{4a}$$

$$M_2 = -D_1 \left( \frac{\partial^2 u_3}{\partial x_1^2} + \nu \frac{\partial^2 u_3}{\partial x_2^2} \right) - D_2 \tau \tag{4b}$$

$$M_{12} = D_1 (1 - \nu) \frac{\partial^2 u_3}{\partial x_1 \partial x_2} \tag{4c}$$

$$\tau := \int_{-h/2}^{h/2} x_3 \alpha T dx_3 \tag{5}$$

$$D_1 := \frac{E h^3}{12(1 - \nu^2)}$$

$$D_2 := \frac{E}{1 - \nu}$$

The integration of Eq. 3 eliminates dependence on the in-plane displacements $u_1$ and $u_2$. The term $\tau$ is called "thermal moment," as it measures the moment associated with the through-thickness temperature distribution. The

constant of proportionality $D_2$ ensures the correct units. This is an input parameter which can be fit to optimally model the bending effects of shot peen. In spite of the fact that shot peen distortion is not driven by thermal expansion in actuality, thermoelasticity is a convenient modeling framework which uses familiar physics to apply distributed bending moments (which do not appear in typical plate bending problems). It can be shown from the equilibrium of moments and vertical forces (see [4]) that the moment components obey a single partial differential equation driven by the transverse loading distribution $p_3(x_1, x_2)$:

$$\frac{\partial^2 M_2}{\partial x_1^2} - 2\frac{\partial^2 M_{12}}{\partial x_1 \partial x_2} - \frac{\partial^2 M_1}{\partial x_2^2} = -p_3$$

Plugging the moment components of Eqs. 4 into this equation yields the governing equation for the transverse displacement:

$$\nabla^4 u_3 = \frac{\partial^4 u_3}{\partial x_1^4} + 2\frac{\partial^4 u_3}{\partial x_1^2 \partial x_2^2} + \frac{\partial^4 u_3}{\partial x_2^4} = \frac{1}{D_1}\left(p_3 - D_2 \nabla^2 \tau\right) \tag{6}$$

**B. Integral Formulation**

Energy formulations of mechanics models tend to generate equations which lend themselves to approximate solutions, and appear as integrals of quantities of interest. Variational methods can then be used to translate the integral expressions to governing differential equations. Additionally, agreement between the integral and differential approaches can act as a check of the model's validity. We will employ the principle of minimum potential energy, which states that the difference between internal strain energy and the work done by applied loads should be at a stationary point. In other words, if we can write the total internal strain energy and the work done by applied loads, the calculus of variations can furnish the governing equation. In order to formulate the problem in this way, we must treat the temperature distribution as a load applied to an elastic 3D solid. The generic expression for strain energy stored in an elastic body is

$$U = \frac{1}{2}\int_V \sigma'_{ij}\epsilon_{ij} dV = \frac{1}{2}\int_V C_{ijk\ell}\epsilon_{k\ell}\epsilon_{ij} dV$$

The compliance tensor $C_{ijk\ell}$ here is not associated with the affine thermoelastic stress-strain relation of Eq. 1, as the thermal contributions are viewed as applied loads. Thus, the stress tensor $\sigma'_{ij}$ only accounts for mechanical stresses. Under the assumptions of the Kirchhoff plate, the internal strain energy is

$$U = \frac{1}{2}\int_V \left(\sigma'_{11}\epsilon_{11} + 2\sigma'_{12}\epsilon_{12} + \sigma'_{22}\epsilon_{22}\right) dV$$

The stress components are written in terms of plate strains as

$$\sigma'_{11} = \frac{E}{1-\nu^2}\left(\epsilon_{11} + \nu\epsilon_{22}\right)$$

$$\sigma'_{22} = \frac{E}{1-\nu^2}\left(\epsilon_{22} + \nu\epsilon_{11}\right)$$

$$\sigma'_{12} = \frac{E}{1+\nu}\epsilon_{12}$$

Eliminating stress terms from the plate strain energy, we find that

$$U = \frac{1}{2}\int_A \int_h \frac{E}{1-\nu^2}\left(\epsilon_{11}^2 + 2\nu\epsilon_{11}\epsilon_{22} + \epsilon_{22}^2\right) + \frac{2E}{1+\nu}\epsilon_{12}^2 dx_3 dA$$

We can plug in the strain components of Eqs. 2 and carry out the $x_3$ integration. Given the presence of the in-plane displacements $u_1$ and $u_2$, this expression for strain energy is very long. It can be seen, however, that there is no coupling between the transverse and in-plane displacements, meaning that $u_3$ and its derivatives do not multiply $u_1$, $u_2$, or their derivatives. The Euler-Lagrange equations used to derive the governing differential equation for bending will cancel terms with no $u_3$ dependence. Thus, writing the energy from bending by only keeping terms involving the transverse displacement $u_3$ will not affect the governing equation for the transverse displacement. The bending strain energy is then

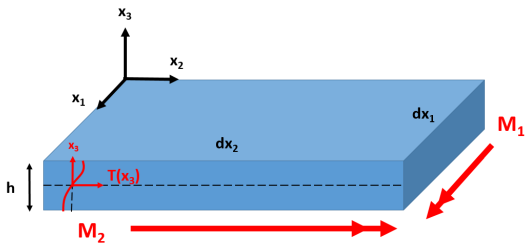


**Fig. 1 Free body diagram of a differential plate element. The moment associated with the temperature distribution is treated as an applied load.**

$$U_b = \int_A \frac{D_1}{2}\left[u_{3,11}^2 + u_{3,22}^2 + 2\nu u_{3,11}u_{3,22} + 2(1-\nu)u_{3,12}^2\right]dA$$

Now we write the work done by the applied transverse pressure and temperature. For simplicity, we impose the requirement $\int \alpha T dx_3 = 0$, which means there is no net in-plane force associated with the temperature distribution. In-plane displacements could be modeled by temperature distributions with associated forces, but here we are only concerned with bending. The work associated with the transverse pressure is simply $\int_A p_3 u_3 dA$, but the thermal moment requires more caution. The work done by a generic torque $T$ is $\int T d\theta$ where $\theta$ is the angle of rotation. Note that the moment components in Figure 1 are moments per span. The differential work done by each of the moment components is then

$$dW_1 = M_1 dx_1 d\Phi_1 = M_1 dx_1 \frac{\partial \Phi_1}{\partial x_2} dx_2$$

$$dW_2 = M_2 dx_2 d\Phi_2 = M_2 dx_2 \frac{\partial \Phi_2}{\partial x_1} dx_1$$

$\Phi_i$ is the angle of rotation around axis $x_i$. Angles of rotation can be approximated by derivatives of the transverse displacement per [4] as $\Phi_1 = u_{3,2}$ and $\Phi_2 = -u_{3,1}$. There is no twisting moment from the temperature distribution, thus the total work done by the two moment components and applied pressure is

$$W = \int_A p_3 u_3 dA + \int_A (dW_1 + dW_2)$$

$$= \int_A p_3 u_3 + M_1 u_{3,22} - M_2 u_{3,11} dA$$

We are assuming that the moment components $M_1$ and $M_2$ from Figure 1 are applied moments, thus they must be related to the thermal moment $\tau$, which models shot peening. We have seen in Eqs. 4 that the magnitude of the moment associated with the temperature distribution is $D_2\tau$. From Eq. 5 and Figure 1, it can be seen that a positive thermal moment corresponds to a negative moment around $x_1$ and a positive moment around $x_2$. Therefore, $M_1 = -D_2\tau$ and $M_2 = D_2\tau$. The work done by the applied pressure and thermal moment is then

$$W = \int_A p_3 u_3 - D_2\tau\left(u_{3,11} + u_{3,22}\right)dA$$

Thus, the difference between the internal bending strain energy $U_b$ and the work done by applied loads $W$ is

$$\Pi = U_b - W = \int_A \frac{D_1}{2}\left(u_{3,11}^2 + u_{3,22}^2 + 2\nu u_{3,11}u_{3,22} + 2(1-\nu)u_{3,12}^2\right) - p_3 u_3 + D_2\tau\left(u_{3,11} + u_{3,22}\right)dA \tag{7}$$

The principle of minimum potential energy says that for a known thermal moment distribution $\tau$ and pressure loading $p_3$, the displacement field $u_3(x_1, x_2)$ will be such that the functional $\Pi$ is at a stationary point. This expression is a functional of the form $\int_A f(u_3, u_{3,11}, u_{3,22}, u_{3,12}, x_1, x_2)dA$, and the corresponding Euler-Lagrange equation is

$$\frac{\partial f}{\partial u_3} + \frac{\partial^2}{\partial x_1^2}\frac{\partial f}{\partial u_{3,11}} + \frac{\partial^2}{\partial x_2^2}\frac{\partial f}{\partial u_{3,22}} + \frac{\partial^2}{\partial x_1 \partial x_2}\frac{\partial f}{\partial u_{3,12}} = 0 \tag{8}$$

Substituting the integrand of $\Pi$ for $f$ in Eq. 8, the governing differential equation is shown to agree with Eq. 6:

$$\nabla^4 u_3 = \frac{1}{D_1}\Big(p_3 - D_2 \nabla^2 \tau\Big) \tag{6}$$

## IV. Moment-Intensity Relation

We wish to design a simple factory test to calculate the thermal moment which best models shot peening at a given intensity. Analogous to a plate with no pressure loading and applied edge moments, assume the displacement field of a plate fully peened at a constant intensity is

$$u_3 = Ax_1^2 + Bx_1x_2 + Cx_2^2$$

where $A$, $B$ and $C$ are constants which depend on the applied moments. Claim that the thermal moment $\tau$ is constant throughout the plate if it is shot peened uniformly, thus $\nabla^2 \tau = 0$. This ansatz solution automatically satisfies the biharmonic equation $\nabla^4 u_3 = 0$. It can be shown from the definition of the moment components given in Eq. 4 that

$$M_1 = D_1\Big(2Av + 2C\Big) + D_2\tau$$

$$M_2 = -D_1\Big(2A + 2Cv\Big) - D_2\tau$$

$$M_{12} = D_1\Big(1 - v\Big)B$$

Assuming that the thermal moment is constant for the case of uniform shot peen, the bending moment components are constant throughout the plate as well. When all the applied edge moments are zero, this is the solution for the displacement field of the plate under thermal loads only. Using the definition of $D_1$ and $D_2$, these equations can be inverted with zero applied edge moment to find

$$A = C = -\frac{6}{h^3}\tau$$

where $B = 0$ because no twisting behavior is induced in the plate from thermal expansion. The displacement field is then

$$u_3 = -\frac{6}{h^3}\tau\Big(x_1^2 + x_2^2\Big)$$

Here, we imagine the origin is at the center of a plate of side lengths $\ell_1$ and $\ell_2$. The thickness $h$ of the test sample should be the same as the plate we wish to model, as the thermal moment associated with shot peen might depend on the plate thickness. However, the side lengths $\ell_1$ and $\ell_2$ can be specific to the test sample. The maximum displacement will be obtained at the corner of the plate, which allows us to calculate the associated moment as

$$|u_{max}| = \frac{3}{2h^3}\tau\Big(\ell_1^2 + \ell_2^2\Big)$$

$$\implies \tau = \frac{2h^3|u_{max}|}{3(\ell_1^2 + \ell_2^2)} \tag{9}$$

Practically speaking, this maximum displacement will be the height a flat plate rises to after being uniformly peened on one side. The value of the thermal moment corresponding to a given shot peen intensity can be calculated with the maximum displacement of a uniformly peened plate. **This calculation relates the shot peen intensity to an equivalent thermal moment $\tau$ via a simple test. The test is used to optimally fit the thermal moment parameter to the actual shot peen process under the assumption that uniform peening gives rise to constant bending moments in the plate.** Whether this line of reasoning leads to accurate predictions of deformation for non-uniform distributions of shot

| Intensity Level | $u_{max}$ | $\tau$ |
|---|---|---|
| 1 | $u_1$ | $\frac{2h^3}{3(\ell_1^2+\ell_2^2)}u_1$ |
| 2 | $u_2$ | $\frac{2h^3}{3(\ell_1^2+\ell_2^2)}u_2$ |
| $\vdots$ | $\vdots$ | $\vdots$ |

**Table 1 Relationship between shot peen intensity and the model input $\tau$ to be generated from tests in the factory.**

peen intensity remains to be seen. It should be assumed that the thermal moment depends on the material and thickness until abundant test data proves otherwise. Thus, in order to calculate the equivalent thermal moment associated with shot peening for a given material and thickness, a series of tests can be carried out where a plate is fully peened at different intensities and the maximum displacement is measured. This displacement is related to the moment $\tau$ and stored as in Table 1.

Intensity is defined as the maximum displacement of a standardized steel “almen" strip after being peened, so for these plates, $u_{max} = I$. Assuming there is still a linear relationship between intensity and displacement for other materials and plate thicknesses, we can write $\tau = KI$ where the constant of proportionality is a combination of the empirical intensity-displacement and the analytical displacement-moment relationships. In this sense, almen strips do not require testing in order to make predictions, as the moment-intensity relation is already known. Note also that the “sign" of the moment can be controlled by shot peening different sides of the plate.

## V. Solution Procedure

### A. Rayleigh-Ritz

We are ready to solve for the transverse displacement field of a shot peened plate now that intensity can be linked to the model input of thermal moment. Given the difficulty of analytically solving Eq. 6 for anything but the simplest boundary conditions (simply supported and clamped edges), we will use the Rayleigh-Ritz procedure [4] to approximate a solution to the plate bending problem. This makes use of the integral formulation of the problem given in Eq. 7. The Rayleigh-Ritz procedure begins by writing the transverse displacement field as an unknown combination of known shape functions:

$$u_3(x_1, x_2) = \sum_{m=0}^{M-1} \sum_{n=0}^{N-1} a_{nm} \phi_n^{(1)}(x_1) \phi_m^{(2)}(x_2) \tag{10}$$

The values $N$ and $M$ are the number of shape functions used in each direction of the approximation, and the sum is chosen to start at zero to align with zero indexing conventions in many programming languages. The shape functions $\phi^{(1)}$ and $\phi^{(2)}$ each depend on one spatial coordinate and are chosen to reflect boundary conditions of the problem at hand. We will first derive a general Rayleigh-Ritz method in terms of the unspecified shape functions, then discuss specific plate support configurations and the corresponding shape functions. Though this double sum is a valid formulation of the transverse displacement, converting to an equivalent single sum will permit a more intuitive matrix-based solution procedure. First, observe that Eq. 10 can be thought of contracting on both indices of the matrices $a_{nm}$ and $\phi_n \phi_m$. By flattening the rows of the matrices, this expression can be written more compactly as

$$u_3(x_1, x_2) = \sum_i a_i \Phi_i = \begin{bmatrix} a_{00} \\ a_{01} \\ \vdots \\ a_{0(M-1)} \\ a_{10} \\ a_{11} \\ \vdots \\ a_{(N-1)(M-1)} \end{bmatrix} \cdot \begin{bmatrix} \phi_0^{(1)} \phi_0^{(2)} \\ \phi_0^{(1)} \phi_1^{(2)} \\ \vdots \\ \phi_0^{(1)} \phi_{M-1}^{(2)} \\ \phi_1^{(1)} \phi_0^{(2)} \\ \phi_1^{(1)} \phi_1^{(2)} \\ \vdots \\ \phi_{N-1}^{(1)} \phi_{M-1}^{(2)} \end{bmatrix}$$

It can be seen that the entries of $\Phi$ comprise the two shape functions in a straightforward way:

$$\Phi_n = \phi^{(1)}_{n//M} \phi^{(2)}_{n\%M} \tag{11}$$

The operators "//" and "%" are the pythonic floor and modular division operators respectively. Having shown that the transverse displacement can be written as a single series, we will assume that the thermal moment distribution can be represented as a series of the same sort. Similarly, if we want to account for transverse loading either from the plate's own weight or explicit applied pressures, the transverse loading distribution must also be represented as a series. The relevant functions are then

$$u_3(x_1, x_2) = \sum_{n=0}^{NM-1} a_n \Phi_n \tag{12a}$$

$$\tau(x_1, x_2) = \sum_{n=0}^{NM-1} t_n \Phi_n \tag{12b}$$

$$p_3(x_1, x_2) = \sum_{n=0}^{NM-1} p_n \Phi_n \tag{12c}$$

Assuming that the pressure and thermal moment distributions are known inputs, we require a means of converting from a typical spatial representation to the series expansion. For an arbitrary known function $f$, the coefficients of the series expansion can be computed by projecting onto the $n$-th shape function and normalizing:

$$f_n = \frac{\int f(x_1, x_2) \Phi_n dA}{\int \Phi_n^2 dA} \tag{13}$$

The loading distributions can then be converted to the required form. Calculating the displacement field of the panel from known loads is the "forward" version of the problem, which we discuss first. Calculating the loads required to obtain a specified shape is the "inverse" problem and will also be discussed. By plugging Eqs. 12 into Eq. 7, the bending strain energy can be written in terms of the coefficients on the transverse displacement $a_n$ and the coefficients governing the known loading distributions. The expression for strain energy is reproduced for reference:

$$\Pi = \int_A \frac{D_1}{2} \Big( u_{3,11}^2 + u_{3,22}^2 + 2\nu u_{3,11} u_{3,22} + 2(1-\nu) u_{3,12}^2 \Big) - p_3 u_3 + D_2 \tau \Big( u_{3,11} + u_{3,22} \Big) dA \tag{7}$$

Each of the terms is calculated by substituting Eqs. 12. For a specified set of shape functions, the definition of $\Phi$ given in Eq. 11 can be used to explicitly carry out the required derivatives and integrations. See Appendix B and C for a sketch of these calculations. The potential energy can be written as the sum of a quadratic and linear form in terms of the vector of coefficients:

$$\Pi = \frac{1}{2} K_{ni} a_n a_i + F_i a_i \tag{14}$$

Choosing to write the displacement field and loading distributions as a single sum leads to a matrix formulation of the potential energy. $K$ is called the stiffness matrix and has known entries. It is the symmetric part of the expression which arises substituting Eqs. 12 into Eq. 7:

$$K_{ni} = \frac{1}{2} \Big( K'_{ni} + K'_{in} \Big)$$

$$K'_{ni} = D_1 \int \int \Big[ \Phi_{n,11} \Phi_{i,11} + \Phi_{n,22} \Phi_{i,22} + 2(1-\nu) \Phi_{n,12} \Phi_{i,12} + 2\nu \Phi_{n,11} \Phi_{i,22} \Big] dx_1 dx_2 \tag{15}$$

Quadratic forms of this sort are unchanged by taking the symmetric part of the matrix, and had we not taken the symmetric part, this expression would have arisen naturally when taking derivatives of the potential energy. The other parameter $F$ is called the load vector and also has known entries:

| $n$ | $P_n(x_1)$ |
|---|---|
| 0 | $1$ |
| 1 | $x$ |
| 2 | $\frac{1}{2}(3x^2-1)$ |
| 3 | $\frac{1}{2}(5x^3-3x)$ |
| 4 | $\frac{1}{8}(35x^4-30x^2+3)$ |
| 5 | $\frac{1}{8}(63x^5-70x^3+15x)$ |
| 6 | $\frac{1}{16}(231x^6-315x^4+105x^2-5)$ |
| 7 | $\frac{1}{16}(429x^7-693x^5+315x^3-35x)$ |

**Table 2 Set of Legendre polynomials up to degree 7. Higher order polynomials can be taken from tabulations or calculated from closed form generating functions.**

$$F_i = \sum_{n=0}^{NM-1} \left[ D_2 t_n \int\int \Big( \Phi_n \Phi_{i,11} + \Phi_n \Phi_{i,22} \Big) dx_1 dx_2 - p_n \int\int \Phi_n \Phi_i dx_1 dx_2 \right] \tag{16}$$

The principle of minimum potential energy requires that the total potential energy, written in the form of Eq. 14, be at a stationary point. This requires that

$$\begin{aligned} \frac{\partial \Pi}{\partial a_j} &= K_{ji} a_i + F_j = 0 \\ \implies \vec{a} &= -K^{-1} F \end{aligned} \tag{17}$$

The coefficients on the transverse displacement under specified loading conditions are straightforward to obtain once the stiffness matrix $K$ and the load vector $F$ have been constructed. These two parameters depend on the shape functions $\phi^{(1)}$, $\phi^{(2)}$, and the moment/pressure distributions. The shape functions are chosen to reflect the edge support configuration, which in turn affects the type of loading a plate can support. We now discuss a case relevant to the modeling of shot peen formed plates.

## VI. Unconstrained Plate

Figure 2 shows an unconstrained plate which is subject to thermal moment only. This scenario does not allow for pressure loading because there are no edge supports to provide vertical reaction forces, and there are no geometric boundary conditions to impose on the shape functions. This setup models a shot peened sample resting on a flat surface. So long as the effect of the part's weight is small compared to the applied moments from peening, this will be a very realistic model for many parts. We choose Legendre polynomials as shape functions for the free edges, as they are bounded and have either even/odd behavior on their domain with no restrictions on the displacement or slope at the boundaries. Thus, Eq. 11 for the unconstrained part becomes

$$\Phi_n = P_{n//M}\left( \frac{x_1 - L_1/2}{L_1/2} \right) P_{n\%M}\left( \frac{x_2 - L_2/2}{L_2/2} \right)$$

Because typical Legendre polynomials are defined on the interval $[-1, 1]$, we must perform a simple coordinate transformation to match the plate geometry. Obtaining a solution for a plate with four free edges requires some additional developments beyond the generalized Rayleigh-Ritz procedure. There are three rigid body shape functions in this set of Legendre polynomials: 1, $\frac{x_1 - L_1/2}{L_1/2}$ and $\frac{x_2 - L_2/2}{L_2/2}$. These functions do not contribute to the strain energy because they represent one rigid body translation and two rotations respectively. The effect of this is to make the stiffness matrix in Eq. 17 not invertible. The lack of geometric boundary conditions require us to "manually" orient the transverse displacement field in space, effectively removing the unconstrained rigid body modes. These added constraints can be enforced with Lagrange multipliers. The new problem requires minimizing Eq. 14 subject to three conditions on the transverse displacement. For convenience, we will choose to zero the displacement at three corners: $u_3(0,0) = u_3(L_1, 0) = u_3(0, L_2) = 0$. Using the series representation of the displacement for the unconstrained plate, these constraints read

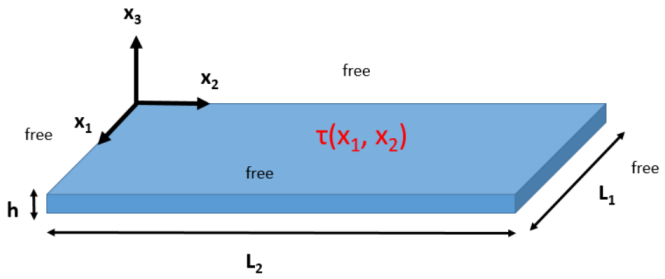


**Fig. 2 A fully unconstrained plate with applied thermal moment and no pressure loading. This is a model for a small peened sample resting on a table.**

$$u_3(0,0) = \sum_n a_n P_{n//M}(-1) P_{n\%M}(-1) = \sum_n a_n (-1)^{n//M} (-1)^{n\%M}$$

$$u_3(L_1,0) = \sum_n a_n P_{n//M}(1) P_{n\%M}(-1) = \sum_n a_n (-1)^{n\%M}$$

$$u_3(0,L_2) = \sum_n a_n P_{n//M}(-1) P_{n\%M}(1) = \sum_n a_n (-1)^{n//M}$$

The boundary properties of the Legendre polynomials make these expressions fairly simple. Following the Lagrange multipliers procedure per [5], the function whose minimum we seek is

$$f(\vec{a},\vec{\lambda}) = \frac{1}{2} K_{ni} a_n a_i + F_i a_i + \lambda_1 \sum a_n (-1)^{n//M} (-1)^{n\%M} + \lambda_2 \sum a_n (-1)^{n\%M} + \lambda_3 \sum a_n (-1)^{n//M} \tag{18}$$

Setting the gradient with respect to the coefficients $\vec{a}$ and the Lagrange multipliers $\vec{\lambda}$ to zero, we can find the minimum of the potential energy subject to the specified displacement constraints. The relevant derivatives are

$$\frac{\partial f}{\partial a_j} = K_{ji} a_i + F_j + \lambda_1 (-1)^{j//M} (-1)^{j\%M} + \lambda_2 (-1)^{j\%M} + \lambda_3 (-1)^{j//M}$$

$$\frac{\partial f}{\partial \lambda_1} = \sum a_n (-1)^{n//M} (-1)^{n\%M} = \vec{g}_1 \cdot \vec{a}$$

$$\frac{\partial f}{\partial \lambda_2} = \sum a_n (-1)^{n\%M} = \vec{g}_2 \cdot \vec{a}$$

$$\frac{\partial f}{\partial \lambda_3} = \sum a_n (-1)^{n//M} = \vec{g}_3 \cdot \vec{a}$$

where the final equality in the $\lambda$ derivatives defines the entries of the $g$ vectors. We now construct an expanded stiffness matrix which incorporates the constraints by assembling these equations, when set to zero, into a single system. The matrix equation for the expanded system is

$$\begin{bmatrix} K & G \\ G^T & 0 \end{bmatrix} \begin{bmatrix} \vec{a} \\ \vec{\lambda} \end{bmatrix} = \begin{bmatrix} \vec{F} \\ \vec{0} \end{bmatrix} \tag{19}$$

The matrix $G$ is simply $[\vec{g}_1, \vec{g}_2, \vec{g}_3]$, which is used to zero the three corners. The coefficients on the transverse displacement can be calculated by populating and inverting this expanded stiffness matrix. The Lagrange multipliers have been used to assemble this new stiffness matrix which incorporates the three displacement constraints, but their values are not of interest. Calculations of the entries of the regular stiffness matrix and load vector for the two Legendre polynomial shape functions are shown in Appendix C.

## VII. Inverse Problem

Because the principle of minimum potential energy states that the displacement of the plate is such that the energy is at a minimum with respect to the applied loads, Eq. 17 furnishes the load-displacement relation regardless of which is known. Previously, we have treated thermal and pressure loading as known inputs, and the displacement field as the unknown response. The load-displacement relation, however, is equally valid in both directions, meaning that we could input a known displacement field to solve for the required loads. While theoretically valid, experience dictates that this method is unstable and impractical. One reason is that multiple shot peen distributions can generate the same shape. Additionally, unlike the forward version of the problem, it is difficult to determine what a “reasonable" input is. For example, if the transverse displacement is specified at three colinear points on the plate, an interpolation can be used to construct the full displacement field. A linear interpolation will fit a triangular shape, while a polynomial interpolation could smoothly fit the points. The loads required to achieve these two displacement fields will be very different, and entirely dependent on the nature of the interpolation. Additionally, functions which are not informed by the physics of plate bending will require very large loads to generate, even if the displacements themselves are not large. Thus, we look for a method which calculates “optimal" thermal loads which generate a displacement field passing through a small number of specified points. The optimality condition will be discussed shortly. For the inverse problem, we restrict ourselves to thermal loading only, and unconstrained parts. This models small, free parts where no displacement constraints are imposed on the edges and the part’s weight is negligible.

When neglecting pressure loading, the load vector in Eq. 17 can be decomposed into a matrix-vector product. Additionally, for the unconstrained plate, the load-displacement relation includes the Lagrange multipliers zeroing three corners. A more compact statement of Eq. 19 makes the dependence on the thermal moment more explicit:

$$\begin{bmatrix} K & G \\ G^T & 0 \end{bmatrix} \begin{bmatrix} \vec{a} \\ \vec{\lambda} \end{bmatrix} = \begin{bmatrix} -T^T \vec{t} \\ \vec{0} \end{bmatrix} = \Gamma \vec{t} \tag{19}$$

$T^T$ is the matrix which takes the coefficients on the thermal moment $\vec{t}$ to the load vector per Eq. 16. $\Gamma$ is the matrix $-T^T$ with three rows of zero appended to the bottom, and is introduced to isolate the moment coefficients. We also introduce a truncation operator $S$, which takes a vector of length $NM + 3$ to length $NM$ by removing the final three entries. This operator has a simple matrix representation and is used to rid of the Lagrange multipliers. The displacement coefficients are then written as a function of the thermal moment:

$$\vec{a} = S \begin{bmatrix} K & G \\ G^T & 0 \end{bmatrix}^{-1} \Gamma \vec{t} \tag{20}$$

Assuming that the displacement field is to be fixed at $P$ points, we use the series representation of the displacement to write the constraints as

$$\sum_j a_j \Phi_j(\vec{x}_1) = u_1, \ldots, \sum_j a_j \Phi_j(\vec{x}_P) = u_P$$

This system of equations can be cast in matrix form by defining the matrix $Q_{ij} = \Phi_j(\vec{x}_i)$. The constraint equations read

$$\vec{u} = Q\vec{a} \tag{21}$$

Finally, use $\kappa$ to denote the inverse of the expanded system matrix in Eq. 20. The constraints can then be written as a function of the moment coefficients via a series of matrix operators:

$$\vec{u} = QS\kappa\Gamma\vec{t} \tag{22}$$

Having written the displacement constraints in terms of the thermal moment, we can now properly formulate the inverse problem. We seek to minimize some function of $\tau$ subject to Eq. 22. This function of $\tau$ determines the nature of the loads which the method generates, and we seek a set of loads which is optimal from a practical standpoint. In the factory, we cannot apply arbitrarily large shot peen intensities, nor arbitrary intensity distributions. The optimal shot peen distribution is both small in magnitude and as close to constant as possible. This suggests choosing a norm which

penalizes large values of both $\tau$ and its derivatives. The chosen norm takes combinations of the square of the thermal moment and all its derivatives up to second order:

$$||\tau|| = \frac{1}{2}\int_A \left[\tau^2 + L_1 L_2\left(\left(\frac{\partial \tau}{\partial x_1}\right)^2 + \left(\frac{\partial \tau}{\partial x_2}\right)^2\right) + L_1^2 L_2^2\left(\left(\frac{\partial^2 \tau}{\partial x_1^2}\right)^2 + \left(\frac{\partial^2 \tau}{\partial x_2^2}\right)^2 + 2\left(\frac{\partial^2 \tau}{\partial x_1 \partial x_2}\right)^2\right)\right] dA \tag{23}$$

where the factor of $\frac{1}{2}$ is introduced to simplify following calculations. The plate side lengths are used somewhat arbitrarily to weight the derivatives differently and to normalize units. This is similar to the H2 norm from the study of partial differential equations. Using the series representation, this expression becomes

$$||\tau|| = \frac{1}{2}\sum_i \sum_j t_i t_j \int_A \left[\Phi_i \Phi_j + L_1 L_2\left(\Phi_{i,1}\Phi_{j,1} + \Phi_{i,2}\Phi_{j,2}\right) + L_1^2 L_2^2\left(\Phi_{i,11}\Phi_{j,11} + \Phi_{i,22}\Phi_{j,22} + 2\Phi_{i,12}\Phi_{j,12}\right)\right] dA \tag{24}$$

which is a quadratic form in the thermal moment. Call the matrix which specifies the norm $H$, so that the right side of Eq. 24 is simply $\frac{1}{2} t_i H_{ij} t_j$. Thus, we seek a minimum to the norm of $\tau$ subject to the constraint that the loads give rise to $P$ specified displacements. The method of Lagrange multipliers states that we minimize the new function

$$f(\vec{t}, \vec{\lambda}) = \frac{1}{2}\vec{t}^T H \vec{t} + \vec{\lambda} \cdot \left(QS\kappa\Gamma\vec{t} - \vec{u}\right) \tag{25}$$

We set the gradient of this function to zero to obtain the condition for a minimum, which will be another linear system. Derivatives are easily calculated using index notation, but are written as matrix equations for readability:

$$\frac{\partial f}{\partial \vec{t}} = H\vec{t} + \left(QS\kappa\Gamma\right)^T \vec{\lambda} = 0$$

$$\frac{\partial f}{\partial \vec{\lambda}} = QS\kappa\Gamma\vec{t} - \vec{u} = 0$$

The two systems of equations can be combined into a single system using block matrices as has been done previously:

$$\begin{bmatrix} H & \left(QS\kappa\Gamma\right)^T \\ QS\kappa\Gamma & 0 \end{bmatrix} \begin{bmatrix} \vec{t} \\ \vec{\lambda} \end{bmatrix} = \begin{bmatrix} \vec{0} \\ \vec{u} \end{bmatrix} \tag{26}$$

The coefficients on the thermal moment can be calculated by inverting the expanded system matrix, and ignoring the values of the Lagrange multipliers. It is stated without proof that invertibility issues will be introduced when the number of constraints on the displacement field becomes large. The problem of interest, however, is to generate loads which are reproducible in the factory and give rise to a small number of specified displacements for an unconstrained panel.

## VIII. Software

Though the derivation of a governing equation for plate bending mirrors that of most solid mechanics models–kinematic assumptions and constitutive relations plugged into equilibrium equations–the required integrations and algebraic manipulations are laborious. The symbolic computation software SageMath has been used to facilitate these mathematical operations, as the addition of a thermal term serves to further complicate the intermediate steps leading to the relatively simple governing equations for bending. The strain components can be defined in terms of displacements, stresses in terms of strains, and energy in terms of stress/strain. Sage carries out the necessary substitutions and simplifies the result. In the following section, Python has been used to convert loading distributions into series expansions (Eq. 13), populate the stiffness matrix and load vector (Eqs. 15 and 16), perform the matrix operations to obtain the displacement coefficients (Eqs. 17 and 19), and to graph/interrogate the results. Numerical integration in the form of Gaussian quadrature was also implemented in Python to reduce the time required to carry out the computations of Appendix C. See Appendix D for a brief discussion of the quadrature routine.

| Parameter | Symbol | Nominal Value | Units |
|---|---|---|---|
| Side Length 1 | $L_1$ | 8.00 | in |
| Side Length 2 | $L_2$ | 8.00 | in |
| Thickness | $h$ | 0.123 | in |
| Young's Modulus | $E$ | 1E7 | psi |
| Poisson's Ratio | $v$ | 0.33 | – |

**Table 3 Nominal values of parameters used for shot peen testing of 6061 T6 AMS 4027 aluminum sheet. Material constants taken from BDM-4085.**

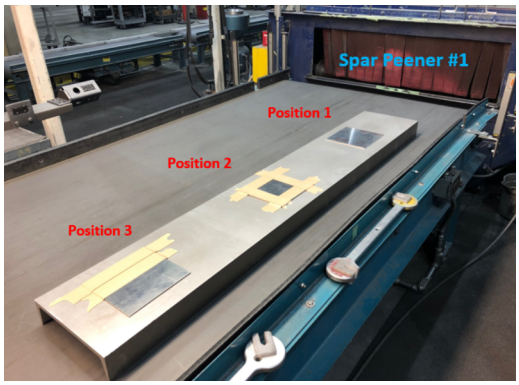


**Fig. 3 Double-sided tape attaches each sample to the holding fixture, which is carried through the machine on a belt. Rubber tape used for shot peen masking seen on the latter two samples.**

## IX. Tests and Implementation

### A. Setup

We seek to compare theoretical predictions to real shot peen forming operations by carrying out factory tests. Test and measurement conditions will be chosen to reflect the conditions of an unconstrained plate. All shot peening is performed on "Spar Peener # 1" using 0.028 inch shot at Frederickson Skin & Spar. An existing shot peen program called "JL PVT 8(6-13) & 8-13" will be used, which is known to peen exposed surfaces at an intensity of 0.0101A. As will be seen, different intensity distributions will be built up with this program and masking, which prevents regions from being peened by applying a rubbery tape. Samples were cut out of a single large sheet of 1/8 in 6061 T6 aluminum. Micrometers were used to check the thickness in the samples, and 0.123 in was determined to be a more accurate estimate. The size of the samples used in testing was chosen to be 8 in square, which maximized the number of available samples while ensuring easily observable and measurable deformations. This material was selected because of its availability in the factory, not because it is a commonly shot peen formed material. This fact is immaterial to the extent that we are testing a general model for shot peen which only makes reference to the material through the assumption of isotropy and the material constants.

Samples will be run through the machine on a long U-shaped fixture three at a time. Double sided tape is used to attach the samples to the flat surface of the fixture, which is selected to prevent shot from piling up inside the channel. Small parts must be mounted on a fixture to avoid falling through wide grates inside the machine, and firmly secured to avoid being "blown away" by the shot stream. The double sided tape was chosen because it is simple, it mimics free boundary conditions, and because it constrains the sample entirely from below (no clamps extending into peened surface).

### B. Measurements

A number of tools are used to take the required measurements. Clamp-type micrometers are used to measure plate thicknesses, and digital calipers are used for the side lengths. In order to measure the maximum displacement of the

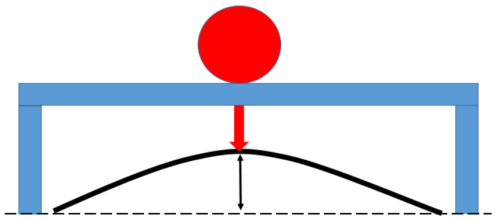

**Fig. 4 Schematic of height gauge measurement system. The measurement reading is the distance from the table to the top of the plate.**

peened samples, we use a digital height gauge on a flat granite table. Figure 4 shows a cross-section of the set-up. A spring-loaded probe extends downwards from mounting blocks of known height until contacting the formed plate. Using the dimensions of the blocks, the distance from the table to the top of the plate is measured. In practice, the approximate center of the sample will be marked, and the probe will be slid around this center-point until the maximum displacement is located. This height gauge method can also be used to estimate flatness of the test plates by measuring the height of un-peened plates and subtracting off the thickness.

It is noted that the theoretical model deals with the displacement of the midplane of the plate, thus the height gauge does not measure the same quantity that the Rayleigh-Ritz method predicts. A simple relationship can be devised to relate the theoretical and measured quantities. Figure 5 shows an $x_2$ slice of a plate of thickness $h$ with the midplane shown as a dashed line. By the Kirchoff plate assumptions, the normal material line remains perpendicular to the midplane as shown at the edge. The measurement $M$ goes from the table to the top of the plate, whereas the theoretical prediction $P$ is the displacement of the midplane. The distance $d$ from the table to the midplane at the plate's edge is less than half the thickness because of the rotation of the edge. It is clear that the theoretical prediction and the measurement are related by

$$d + P + h/2 = M$$

Now, note that the edge will be rotated around both the $x_1$ and $x_2$ axes, so that there exists a second angle of rotation $\alpha_2$ which is not shown in the figure. Practically, it is known that these angles will be small, but the theoretical model can be used to estimate their values more precisely. Projecting the rotated edge onto the vertical axis, we can write

$$d = \frac{h}{2}\cos\alpha_1\cos\alpha_2 \approx \frac{h}{2}\left(1 - \frac{\alpha_1^2}{2}\right)\left(1 - \frac{\alpha_2^2}{2}\right)$$

Cosines have been replaced with a two term Taylor series–a very accurate approximation for small angles. Expanding the multiplication, we neglect the highest order terms to find

$$d \approx \frac{h}{2}\left(1 - \frac{\alpha_1^2}{2} - \frac{\alpha_2^2}{2}\right) = \frac{h}{2} - \frac{h}{4}\left(\alpha_1^2 + \alpha_2^2\right)$$

Because the rotation angles are small, the sum of their squares can also be neglected. Thus, the distance $d$ is accurately approximated by half the thickness. Returning to the relationship between the theoretical prediction and the measurement, this means that

$$P = M - h \tag{27}$$

In summary, the measurement is related to the theoretical midplane displacement by the plate's thickness.

### C. Experimental Design

Per the theoretical approach derived above, samples must be uniformly peened to calculate the associated model input of thermal moment. With the "JL PVT 8(6-13) & 8-13" program shooting at 0.0101A intensity and masking, we construct three non-uniform intensity distributions by which the model can be assessed. Parsimony governed the choice

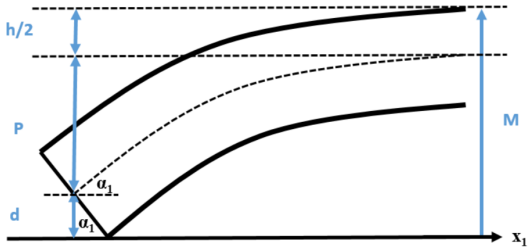


**Fig. 5 Cross section of a formed plate showing the relationship between measured and theoretical quantities.**

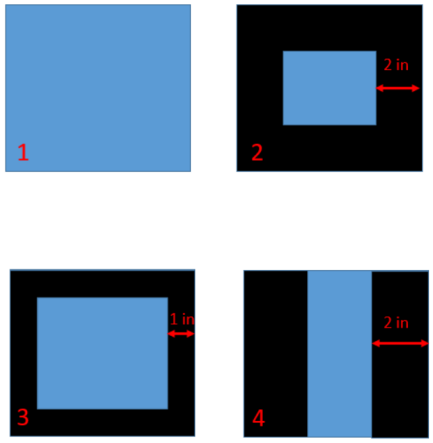


**Fig. 6 Shot peen distributions used in the tests are numbered for reference. Black indicates a masked region of the sample, whereas blue is peened. Masking is a accomplished with one and two inch tape. Configuration 1 is used to calibrate the thermal model, whereas the other configurations can be compared to theoretical predictions.**

| Sample | Run | Position | Configuration |
|---|---|---|---|
| 1 | 1 | 1 | 1 |
| 2 | 1 | 2 | 1 |
| 3 | 1 | 3 | 1 |
| 4 | 2 | 1 | 4 |
| 5 | 2 | 2 | 3 |
| 6 | 2 | 3 | 2 |
| 7 | 3 | 1 | 2 |
| 8 | 3 | 2 | 4 |
| 9 | 3 | 3 | 3 |
| 10 | 4 | 1 | 1 |
| 11 | 4 | 2 | 1 |
| 12 | 4 | 3 | 1 |
| 13 | 5 | 1 | 3 |
| 14 | 5 | 2 | 2 |
| 15 | 5 | 3 | 4 |
| 16 | 6 | 1 | 1 |
| 17 | 6 | 2 | 1 |
| 18 | 6 | 3 | 1 |

**Table 4 Each sample is given a number for identification. The experiment is split into blocks by run number.**

to use a single shot peen program/intensity; both from the standpoint of testing logistics and the forthcoming uncertainty quantification. The configurations used in the tests are shown in Figure 6. The rubber tape used for masking is available in one and two inch widths, so these configurations were selected to be convenient, but also repeatable. For example, a two inch square section of tape could be used to mask the center of the sample, but this would require accurately locating the center and orienting the square. For the configurations of Figure 6, the edges of the samples are used to index the applied masking and no measurements are required. Note that masking does not constrain the plates used in the experiment. Constraints would appear physically as clamping or pinning the edges of samples, and mathematically as boundary conditions. The masking acts only to create non-uniform distributions of shot peen, which can be used to assess the theoretical model calibrated with Eq. 9 on the the uniformly peened plate of Configuration 1.

Having decided on the nature of the samples, the method of peening, the holding fixture, and the intensity distributions to be tested, we turn to the structure of the experiment itself. Because the fixture in Figure 3 will have to be run multiple times to accommodate a realistic number of samples, run-to-variation in the shot peen conditions is introduced. Furthermore, the position on the holding fixture could influence the shot peen intensity a sample sees within a given run. Our task is to design an experiment which is informed by the theoretical model and these hypothesized sources of variation. Because theoretical predictions are driven by estimates of the thermal moment, we seek confidence in our estimate of this parameter, both in its value and associated uncertainty. A run with all three positions occupied by uniformly peened plates will yield an estimate of position-induced variation, and three runs at a given position will yield an estimate of run-to-run variation. We choose to perform three runs of uniformly peened plates at the three positions to better understand the underlying variation in the experiment. These runs of uniform peening will be at the beginning, middle, and end of the experiment, which is carried out in a single session. Interspersed with the uniform plates are the masked configurations, each of which will be replicated three times. This totals to six runs through the machine and 18 samples. Though we are able to estimate run-to-run and position variation separately, they will be effectively lumped together by running the masked samples under maximally variable conditions. In other words, no two replicates of a certain configuration are peened in the same run, or at the same position between runs. See Table 4 for the summary of the experiment.

**D. Uncertainty Quantification**

To realistically compare theoretical predictions to the test samples, we seek to propagate uncertainty in model inputs through the solution procedure to obtain a range of theoretical predictions. This will estimate the degree to which realistic deviations of the inputs from their nominal values influence the theoretical displacement predictions. To do this, we measure/estimate the variation in the inputs and devise a method to account for this. We begin by listing and discussing the various sources of uncertainty:

- **Side Lengths:** samples are cut with a shear machine out of sheet stock. Measuring dimensions with digital calipers reveals the extent of the variation. It is assumed that the two side lengths are independent of one another and that the samples are perfectly square. The two side lengths of the plate are inputted directly into the thermal model.
- **Thickness:** the thickness can be measured within and among samples to estimate variability. Clamping micrometers yield the desired accuracy, and provide measurements which do not confound thickness and flatness. The thickness of the plate, which is assumed to have no spatial variation, is inputted directly into the thermal model.
- **Thermal Moment:** this parameter is the bridge between shot peen and the theoretical model. It's value is calculated with uniformly peened test plates and Eq. 9. The measured displacements of the uniformly peened plates in the experiment (Table 4) will be influenced by run-to-run and positional variation in the machine. They may also be influenced by variability in the material properties of the plate, the condition of its surface, etc. Many variables which cannot be independently measured will be lumped into the distribution of the measured displacements. The thermal moment calculation makes use of the side lengths and thickness, which are also uncertain to the extent that we have not kept track of the dimensions of particular samples. The thermal moment is inputted directly into the model, and combines variability in the sample dimensions, machine precision, and underlying material response. As will be seen, the thermal moment will be calculated per Eq. 9 by sampling the thickness, side lengths, and max displacement independently. In reality, the displacement of the peened plate is dependent on the side lengths and thickness in some unknown way, but we assume independence in lieu of the dimensions associated with each sample.
- **Masking:** the size of the masked area can vary as a result of inconsistencies in applying the tape. The distance from the edge of the sample to the unmasked area can be measured with digital calipers on a variety of samples. This phenomenon is driven by the tape being imperfectly indexed to the sample's edge, and perhaps by stretching effects. The size of the masked region influences the thermal moment distribution which drives displacement in the model.
- **Measurement:** a simple study can be conducted using the height gauge setup of Figure 4 where the same measurements of peened samples are made by multiple individuals and recorded. The discrepancy in these measurements will be considered measurement error. Measurement errors are not model inputs but act to introduce uncertainty around a theoretical prediction for a given set of inputs.
- **Flatness:** the height gauge can also be used to measure the flatness of unpeened samples. Probing around the plate, we look for heights which are larger than the plate's thickness. It was observed that some samples had significant flatness deviations at their corners ($\approx 0.010$ in), likely from being cut on the shear. Unpeened plates are assumed to be flat and stress-free in the thermal model, so flatness is not an input. It is not clear how to account for the effect of flatness deviations on theoretical predictions.
- **Convergence:** a finite series is used to represent the thermal moment distribution and the displacement field, thus truncation error is introduced. The extent of convergence error can be estimated by observing the change in the displacement field under specified shot peen conditions as the number of shape functions increases. The highest order Legendre polynomial used in the representation is degree 11, so small changes in the displacement field before degree 11 indicate adequate convergence. See Figure 7. We use a normalized L1 norm $\left(||f|| = \frac{1}{A}\int |f| dA\right)$ and calculate the norm of the difference of displacement fields of adjacent orders. This is equivalent to calculating the pointwise average change in displacement as the order of the approximation is increased. We can also plot the change in the maximum displacement between approximations of adjacent orders. The number of shape functions in each coordinate direction is equivalent for simplicity.
- **Assumptions:** it has been assumed that the 6061 T6 aluminum is isotropic, that the material constants are known exactly, that the tensile and compressive modulus are equivalent, that the thickness is constant, that the samples are perfectly square, that small flatness deviations do not meaningfully affect the physics of bending, that shot peen does not change the thickness of the sample, that changes in sample length dimensions from peening are

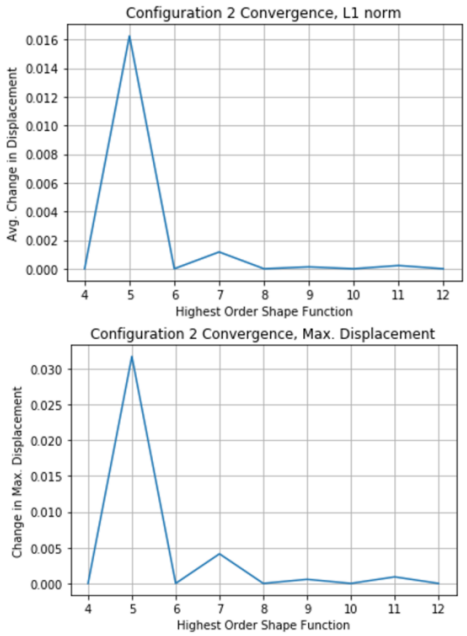


**Fig. 7 Convergence of the model to itself. Plots show two measures of change in the displacement field as the highest order of the two shape functions increases. After degree 8, refining the approximation has little effect on the solution by both measures. Nearly identical behavior is observed for Configurations 3 and 4.**

negligible, that overspray shot peen on the edges of the plate has no effect, and most importantly, that plasticity can be neglected by viewing shot peen forming as the application of distributed torques modeled by applied temperatures. As we either cannot or have not accounted for the effect of these assumptions, the comparison of the experimental results to theoretical predictions will determine to what degree they are reasonable.

We will numerically generate a distribution of theoretical predictions by using a Monte Carlo method whereby the theoretical model is used to predict the displacement at the center of the sample with inputs sampled from probability distributions. This process is repeated a set number of times, and a distribution of predictions is made for each intensity configuration used in the tests. See Table 5 for the sources of variation which are accounted for in this way. It is assumed that each parameter is uniformly distributed around its nominal value with an error that is either measured or estimated. Note that the side length and thickness values used to calculate the thermal moment will be sampled independent of the dimensions of the plate whose displacement we predict. The displacement used in Eq. 9 will be sampled from a uniform distribution encompassing the full range of displacements measured off the uniformly peened plates. The effect of flatness deviations is difficult to predict, and might be approximated by increasing the magnitude of the measurement error.

### E. Results

An analysis of the test results begins with the uniformly peened plates. Table 6 summarizes the measurements taken from these nine samples. Note that the measurements are not midplane displacements, rather the quantity $M$ in Eq. 27 taken directly from the height gauge. Going forward, we will call this the “measured height." A two-way ANOVA with no replication can be performed for the effects of the run # (rows) and position (columns). At a 10% significance level, the null hypothesis of no row effect is rejected, indicating the existence of the assumed run-to-run variation. The column effect is not significant, meaning this data suggests the position on the fixture has no meaningful effect. The maximum displacement used in the Rayleigh-Ritz procedure and Eq. 9 will be generated by sampling a thickness value, and subtracting it from a measurement sampled uniformly from the range $M \in [0.302, 0.311]$. This same thickness, in addition to the independently sampled length dimensions, will be used to calculate the thermal moment at the beginning of each run in the Monte Carlo method. Similarly, the dimensions of the sample and the size of the masked region will be sampled to calculate a theoretical midplane displacement. The thickness used in this calculation will be added to the midplane displacement per Eq. 27 along with a measurement error. In this way, we

| Parameter | Nominal | Error |
|---|---|---|
| Thermal Moment | – | – |
| Side Length 1 | 8.000 | ± 0.025 |
| Side Length 2 | 8.000 | ± 0.025 |
| Thickness | 0.123 | ± 0.0015 |
| Masking | 0.000 | ± 0.050 |
| Measurement | 0.000 | ± 0.001 |

**Table 5 Sources of variation accounted for in the Monte Carlo method of quantifying uncertainty in the theoretical predictions. The nominal value and error of the thermal moment depend on the results of the tests and Eq. 9. Masking error refers to the deviation from the nominal tape widths used to generate the non-trivial intensity distributions.**

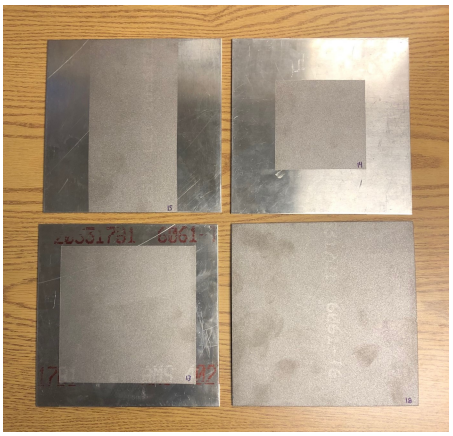

**Fig. 8 Appearance of the samples when peened per the four configurations used in the experiment.**

| | | Position | | |
|---|---|---|---|---|
| | | 1 | 2 | 3 |
| Run | 1 | 0.311 | 0.302 | 0.311 |
| | 4 | 0.301 | 0.300 | 0.300 |
| | 6 | 0.304 | 0.306 | 0.307 |

**Table 6 Measurements taken from the height gauge of the nine uniformly peened plates used to calculate the thermal moment and estimate machine variability. This data indicates that positional variation is less than run-to-run variation.**

| Config. | Sample # | Measurement |
|---|---|---|
| 2 | 6 | 0.207 |
| | 7 | 0.212 |
| | 14 | 0.198 |
| 3 | 5 | 0.252 |
| | 9 | 0.264 |
| | 13 | 0.257 |
| 4 | 4 | 0.254 |
| | 8 | 0.249 |
| | 15 | 0.227 |

**Table 7 Measurements taken from height gauge of the samples with non-uniform intensity distributions. These values are used in assessing the validity of the thermoelastic model.**

generate a theoretical measured height value which can be compared with the remaining test results. From numerical experimentation, it has been observed that 250 samples ensures that the mean and standard deviation of the Monte Carlo distribution stabilize within 2%. This is true for each of the three non-uniform shot peen configurations. Having thus accounted for the uncertainty surrounding theoretical predictions, we are ready to assess the model against the measurements taken from the non-uniform samples, which are shown in Table 7. See Figure 9 for the distributions of the theoretically predicted measured heights, and Figure 10 for the comparison of these distributions to the results of the experiment. The mean and standard deviation are taken from each of the Monte Carlo distributions, and the error bars in Figure 10 are ± two standard deviations centered at the mean.

### F. Inverse Problem Results

We claim that the inverse method does not introduce new physics to the thermal plate model and thus restrict ourselves to a brief theoretical discussion of its behavior/implementation. In other words, we can rely on the results of the previous section in assessing the likelihood of generating the specified displacements from the predicted thermal moments in practice. Of primary importance is the choice of norm, which should favor “realistic" shot peen distributions. Eq. 23 is a variant of the H2 norm, which simultaneously minimizes the magnitude, slope, and curvature of the thermal

| Specified Displacements | | |
|---|---|---|
| $x_1$ | $x_2$ | $u_3$ |
| 8.00 | 8.00 | 0.000 |
| 4.00 | 4.00 | 0.050 |

**Table 8 A simple test of the inverse method for the unconstrained plate, which takes in displacement values specified at certain points. In this case, we zero the fourth corner of the plate and specify a single displacement in the center.**

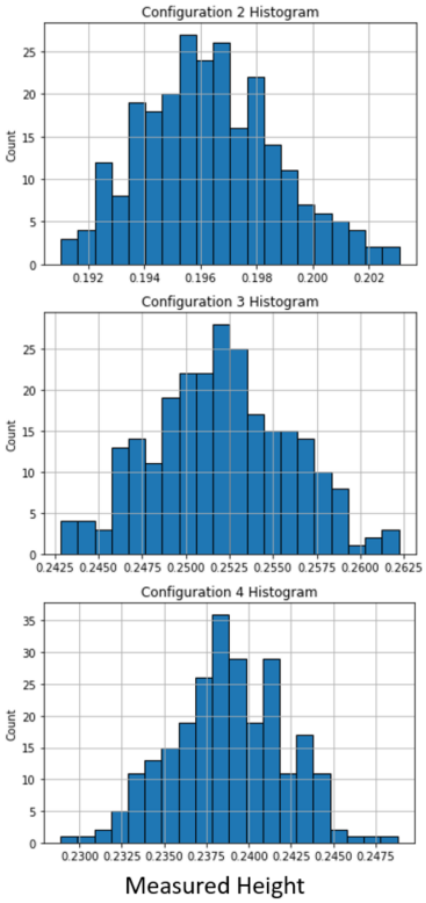


**Fig. 9 Monte Carlo distributions of the three peening configurations generated using 250 samples.**

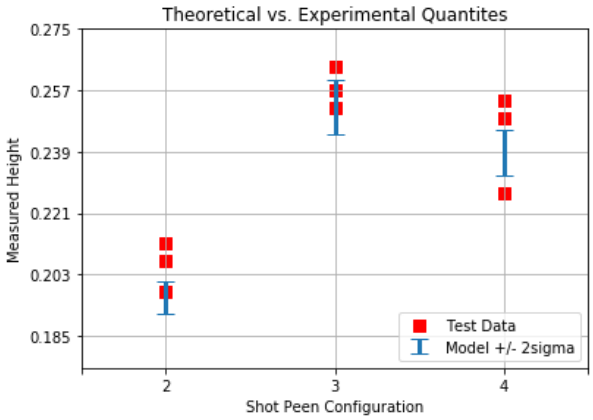


**Fig. 10 Overlay of the theoretical model with uncertainty and results from the experiment.**

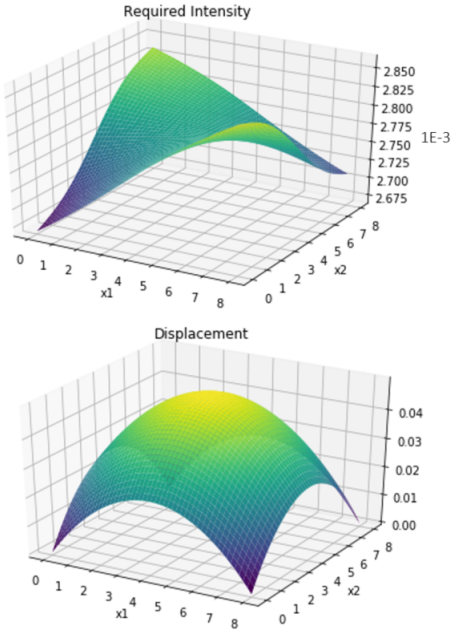


**Fig. 11 The calculated intensity distribution yields a displacement field passing through the specified points, which is small in magnitude, and approximately constant in the interior.**

moment. Table 8 shows the most straightforward test of the inverse method–we seek a method of peening a theoretically exact version of the test sample which gives rise to a certain arc height when resting on a flat surface. Three of the four corners are already zeroed from the Lagrange multipliers, but we must artificially impose the zeroing of the fourth corner. Considering the test results in the previous section, 0.050 in midplane displacement at the center is small and should require a lower intensity than was used in the experiments. However, we do not know the general moment-intensity relation, as it was only calculated at the experimental intensity of 0.0101A. It is clear that zero intensity gives rise to zero displacement, so we will assume a linear relationship for the sake of example. This allows us to write

$$\tau = \frac{2h^3}{3(L_1^2 + L_2^2)} u_{max}(I) = \frac{2h^3}{3(L_1^2 + L_2^2)} \frac{0.182}{0.0101} I$$

where 0.182 is a representative midplane displacement from the test results shown in Table 6, (the average measured height of 0.305 with the nominal plate thickness subtracted off), and the dimensions of the sample are treated as exact. With this relationship, we can avoid discussing predictions of the thermal moment, for which we have little intuition. Figure 11 shows the results of the inverse method using the inputs specified in Table 8 and the norm given in Eq. 23. The shape of the displacement field is approximately spherical and satisfies the imposed constraints. The intensity distribution is smooth and minimally variable. These results suggest that uniformly peening the sample at 0.003A intensity would generate a midplane displacement $\approx 0.050$ in.

## X. Conclusion

We have hypothesized a model for shot peen forming which allows plasticity to be neglected, namely that the forming effect can be modeled with spatially varying elastic moments. A thermoelastic model is derived which supports distributed moments as an input, as this is not a typical input for purely mechanical plate models. A test is devised to calculate the value of this equivalent moment for each shot peen intensity. Then, the Rayleigh-Ritz procedure is developed and implemented in Python in order to solve the thermoelastic equations for boundary conditions relevant to shot peen forming. An inverse method is formulated in order to create shot peen forming recipes from known displacements. Finally, an experiment is designed by which to test the thermoelastic model, and uncertainty estimation is used to compare model predictions to test data more carefully. Figure 10 shows the comparison of the linear thermal model to measurements taken from the test samples. We see that three experimental measurements fell within the range

of uncertainty on the model predictions. Five measurements were larger than the model predictions, and one smaller. The data suggests that the model underestimates the experimental measurements, though for Configuration 4 especially, we notice significant variation underlying the shot peen process. Taking the average of the test data and comparing to the mean theoretical prediction, the model seems to be accurate within 10%. More testing will be required to understand if the observed patterns are true systematic shifts in the model, or unexplained variation in the shot peen process. This will involve using different sample dimensions, materials, and more replication. Additionally, future tests might overlay multiple shot peen intensities, via multiple runs through the machine, to assess the model in this more general scenario. Further experimentation might also focus on validating/implementing the inverse method.

## References


[1] Koch, W. J., "Peen forming predictions using finite element analysis," Seattle, WA: Applied Research and Technology, 1997.

[2] Wang, T., Platts, M. J., and Levers, A., "A process model for shot peen forming," Journal of Materials Processing Technology, vol. 172, 2006, pp. 159–162.

[3] Nervi, S., and Castle, J., "Modeling the Effects of Surface Residual Stresses: A simple model for the computation of distortion on thin monolithic aerospace components," Boeing Technical Journal, vol. 3, Dec. 2013.

[4] Bauchau O. A., and Craig J.I., "Kirchhoff Plate Theory," Structural Analysis: With Applications to Aerospace Structures, Springer, 2016, pp. 819–865.

[5] Marsden, J. E., and Tromba, A., "Vector calculus," New York, NY: W.H. Freeman, 2012, pp. 230–250.

[6] Hansen, E. W., "Fourier Transforms: Principles and Applications," With an Introduction to Complex Analysis, Hoboken: John Wiley, 2015.

[7] Ugural, A. C., and Fenster, S. K., "Two Dimensional Problems in Elasticity," Advanced Strength and Applied Elasticity, Upper Saddle River, NJ: Prentice Hall, 2012, pp. 95–135.

[8] Griffiths, D. J., "Introduction to electrodynamics," Cambridge , MA: Cambridge University Press, 2018, pp. 140–160.


## A. Appendix A - Orthogonality Relation

$$\int_0^L P_n\left(\frac{x-L/2}{L/2}\right)P_m\left(\frac{x-L/2}{L/2}\right)dx = \frac{L}{2}\int_{-}^{} 1^1 P_n(u)P_m(u)du$$

$$= \frac{L}{2n+1}\delta_{nm} =: \delta_P(n,m)$$

## B. Appendix B - Term Calculations

- $\int u_{3,11}^2 dA = \sum_{n=0}^{NM-1}\sum_{i=0}^{NM-1} a_n a_i \int\int \Phi_{n,11}\Phi_{i,11}dx_1dx_2$
- $\int u_{3,22}^2 dA = \sum_{n=0}^{NM-1}\sum_{i=0}^{NM-1} a_n a_i \int\int \Phi_{n,22}\Phi_{i,22}dx_1dx_2$
- $\int u_{3,12}^2 dA = \sum_{n=0}^{NM-1}\sum_{i=0}^{NM-1} a_n a_i \int\int \Phi_{n,12}\Phi_{i,12}dx_1dx_2$
- $\int u_{3,11}u_{3,22} dA = \sum_{n=0}^{NM-1}\sum_{i=0}^{NM-1} a_n a_i \int\int \Phi_{n,11}\Phi_{i,22}dx_1dx_2$
- $\int p_3 u_3 dA = \sum_{n=0}^{NM-1}\sum_{i=0}^{NM-1} p_n a_i \int\int \Phi_n\Phi_i dx_1dx_2$

$$\bullet \int \tau\Big(u_{3,11} + u_{3,22}\Big)dA = \sum_{n=0}^{NM-1}\sum_{i=0}^{NM-1} t_n a_i \int\int \Big(\Phi_n\Phi_{i,11} + \Phi_n\Phi_{i,22}\Big)dx_1 dx_2$$

## C. Appendix C - Integral Calculations

The terms used to construct the load vector and stiffness matrix are calculated for the two support configurations. Integrals over $x_1$ range from 0 to $L_1$, and similarly for $x_2$. Orthogonality of the shape functions is used so that zeros can be enforced without carrying out the integrals. Note that derivatives of Legendre polynomials are not themselves Legendre polynomials, thus orthogonality does not apply.

$$\bullet \int \Phi_{n,11}\Phi_{i,11}dA = \int \frac{\partial^2}{\partial x_1^2}P_{n//M}\frac{\partial^2}{\partial x_1^2}P_{i//M}dx_1 \int P_{n\%M}P_{i\%M}dx_2$$

$$= \left(\int \frac{\partial^2}{\partial x_1^2}P_{n//M}\frac{\partial^2}{\partial x_1^2}P_{i//M}dx_1\right)\delta_P(n\%M, i\%M)$$

$$\bullet \int \Phi_{n,22}\Phi_{i,22}dA = \int P_{n//M}P_{i//M}dx_1 \int \frac{\partial^2}{\partial x_1^2}P_{n\%M}\frac{\partial^2}{\partial x_1^2}P_{i\%M}dx_2$$

$$= \delta_P(n//M, i//M)\left(\int \frac{\partial^2}{\partial x_1^2}P_{n\%M}\frac{\partial^2}{\partial x_1^2}P_{i\%M}dx_2\right)$$

$$\bullet \int \Phi_{n,12}\Phi_{i,12}dA = \int \frac{\partial}{\partial x_1}P_{n//M}\frac{\partial}{\partial x_1}P_{i//M}dx_1 \int \frac{\partial}{\partial x_2}P_{n\%M}\frac{\partial}{\partial x_2}P_{i\%M}dx_2$$

$$\bullet \int \Phi_{n,11}\Phi_{i,22}dA = \int \frac{\partial^2}{\partial x_1^2}P_{n//M}P_{i//M}dx_1 \int P_{n\%M}\frac{\partial^2}{\partial x_2^2}P_{i\%M}dx_2$$

$$\bullet \int \Phi_n\Phi_i dA = \int P_{n//M}P_{i//M}dx_1 \int P_{n\%M}P_{i\%M}dx_2$$

$$= \delta_P(n//M, i//M)\delta_P(n\%M, i\%M)$$

$$\bullet \int \Phi_n\Phi_{i,11}dA = \int P_{n//M}\frac{\partial^2}{\partial x_1^2}P_{i//M}dx_1 \int P_{n\%M}P_{i\%M}dx_2$$

$$= \left(\int P_{n//M}\frac{\partial^2}{\partial x_1^2}P_{i//M}dx_1\right)\delta_P(n\%M, i\%M)$$

$$\bullet \int \Phi_n\Phi_{i,22}dA = \int P_{n//M}P_{i//M}dx_1 \int P_{n\%M}\frac{\partial^2}{\partial x_2^2}P_{i\%M}dx_2$$

$$= \delta_P(n//M, i//M)\left(\int P_{n\%M}\frac{\partial^2}{\partial x_2^2}P_{i\%M}dx_2\right)$$

## D. Appendix D - Gaussian Quadrature

In order to speed up the numerical integration, we make use Gauss-Legendre quadrature. This allows integrals of degree $2n-1$ polynomials to be converted to weighted sums of the polynomial evaluated at $n$ points. Mathematically, this reads

$$\int_0^L f(x)dx = \frac{L}{2}\int_{-1}^{1} f\left(\frac{L}{2}\xi + \frac{L}{2}\right)d\xi = \frac{L}{2}\sum_{i=1}^{n} w_i f\left(\frac{L}{2}\xi_i + \frac{L}{2}\right)$$

The second step makes use of a change of variables to switch the integration region to $[-1, 1]$ over which Gaussian quadrature is typically defined. If $f(x)$ is a polynomial of degree $2n-1$ or less, it can be shown that the equality is exact for the correct choice of weights $w_i$ and integration points $\xi_i$. These values are stored in Python libraries and can be easily called out in a custom integration routine. Thus, integrals of Legendre polynomials and their derivatives can be evaluated exactly as simple algebraic expressions.

## E. Appendix E - FEM Inputs

Though the Rayleigh-Ritz approach facilitates analytical solution to the bending problem, we might also wonder how these results can be transferred to thermal FEA. We can calculate the temperature distribution that best models the thermal moment associated with shot peen at a given intensity. By definition,

$$\tau = KI = \int_{-h/2}^{h/2} x_3 \alpha T dx_3$$

We want to find the temperature distribution $T(x_3)$ which gives rise to this moment. The moment-intensity tests/results are used to associate the thermal moment and shot peen intensity via the constant $K$. Obviously, there isn't a unique solution as the temperature could take many forms while leaving the relevant integral unchanged. Assume that the temperature distribution is linear about the midpoint of the plate, ie $T(x_3) = T_0 x_3$. We can then calculate the slope $T_0$:

$$\tau = \int_{-h/2}^{h/2} \alpha T_0 x_3^2 dx_3 = \frac{\alpha T_0 h^3}{12} \implies T_0 = \frac{12KI}{\alpha h^3}$$

As expected, the slope of the temperature distribution increases with the shot peen intensity. Though the choice of a linear temperature distribution is arbitrary, it might be justified as a way to enforce the assumption of strain which is linearly distributed through the plate thickness, as the Kirchhoff model requires. Thus, a thermoelastic computational model could predict displacements from a given map of shot peen intensity by applying the appropriate boundary conditions and temperature distribution at each point in the plate.